Tectonophysics 658 (2015) 61–73

Contents lists available at ScienceDirect

Tectonophysics

journal homepage: www.elsevier.com/locate/tecto

Three-dimensional estimate of the lithospheric effective elastic thickness of the Line ridge

Minzhang Hu [a,b,*], Jiancheng Li [b], Taoyong Jin [b], Xinyu Xu [b], Lelin Xing [a], Chongyang Shen [a], Hui Li [a,**]

[a] Key Laboratory of Earthquake Geodesy, Institute of Seismology, China Earthquake Administration, 40 Hongshan Celu, Wuhan, China
[b] Institute of Geodesy and Geophysics, School of Geodesy and Geomatics, Wuhan University, 129, Luoyu Road, Wuhan, China

ARTICLE INFO

Article history:
Received 11 December 2014
Received in revised form 11 July 2015
Accepted 16 July 2015
Available online 26 July 2015

Keywords:
Line ridge
Lithosphere
Effective elastic thickness
Flexural isostasy
Admittance

ABSTRACT

Using a new bathymetry grid formed with vertical gravity gradient anomalies and ship soundings (BAT_VGG), a 1° × 1° lithospheric effective elastic thickness (*Te*) grid of the Line ridge was calculated with the moving window admittance technique. As a comparison, both the GEBCO_08 and SIO V15.1 bathymetry datasets were used to calculate *Te* as well. The results show that BAT_VGG is suitable for the calculation of lithospheric effective elastic thickness. The lithospheric effective elastic thickness of the Line ridge is shown to be low, in the range of 5.5–13 km, with an average of 8 km and a standard deviation of 1.3 km. Using the plate cooling model as a reference, most of the effective elastic thicknesses are controlled by the 150–300 °C isotherm. Seamounts are primarily present in two zones, with lithospheric ages of 20–35 Ma and 40–60 Ma, at the time of loading. Unlike the Hawaiian-Emperor chain, the lithospheric effective elastic thickness of the Line ridge does not change monotonously. The tectonic setting of the Line ridge is discussed in detail based on our *Te* results and the seamount ages collected from the literature. The results show that thermal and fracture activities must have played an important role in the origin and evolution of the ridge.

1. Introduction

The effective elastic thickness (*Te*) is sensitive to the thermal–mechanical properties of the lithosphere under the submarine features. The study of *Te* of the lithosphere under seamounts can further our understanding of the evolutionary process of the lithosphere. According to the cooling plate model (Parsons and Sclater, 1977; Stein and Stein, 1992), the strength of the lithosphere should increase with age. Many studies have suggested that the oceanic *Te* is determined to a first order by the age of the lithosphere at the time of loading and is approximately represented by the depth of the 450 ± 150 °C isotherms (Calmant et al., 1990; Watts, 1978, 2001).

The Line ridge is a seamount chain located in the center of the Pacific Ocean, as shown in Fig. 1. The ridge has several branches, such as the Keli Ridge, which formed at nearly the same time as the main chain (Davis et al., 2002). Volcanisms along the ridge do not display linear age progressions, like the Hawaiian-Emperor chain, and can't be attributed to hot spots sustained by deep mantle plumes. The long durations of volcanism and quasi-synchronous activity over great distance call for a more complicated explanation.

Wilson (1963) argued that the seamount chains are caused by "hot spot" activity. The Hawaiian-Emperor chain is a typical example generated by the activity of a single hot spot. At present, the hot spot is situated at the southeast end of the chain. Based on the study of rough bathymetry, Morgan (1972) suggested that the Line ridge, together with the Tuamotu Islands, is a seamount chain generated by a single hot spot, similar to the Hawaiian-Emperor chain. Schlanger et al. (1984) noted that the Line ridge may have been generated by one or more hot spots based on the lithology and age of the seamounts, obtained from the Deep Sea Drilling Project (DSDP). The Line ridge may not have been produce by a single hot spot, like the Hawaiian-Emperor chain. Although the lithology of the seamounts along the Line ridge is similar to the Hawaiian-Emperor chain, there are certain significant differences. First, the geomorphology of the Line ridge is more complex than that of the Hawaiian-Emperor chain and has more distinct branches along the ridge. Second, the ages of the Line ridge seamounts are diverse and irregular.

According to the fracture zones shown in Fig. 1, as well as the magnetic anomaly data to the north of the Line ridge, Nakanishi (1993) inferred that the main chain of the ridge may be parallel to a vanished mid-ocean ridge. Winterer (1976) also suggested that the Line ridge was the product of a mid-ocean ridge. But the hypothesis that the Line ridge was constructed by the activity of a mid-ocean ridge is not

* Correspondence to: M. Hu, Key Laboratory of Earthquake Geodesy, Institute of Seismology, China Earthquake Administration, 40 Hongshan Celu, Wuhan, China.
** Corresponding author.
E-mail addresses: mzhhu@whu.edu.cn (M. Hu), lihuidz@public.wh.hb.cn (H. Li).

http://dx.doi.org/10.1016/j.tecto.2015.07.008
0040-1951/

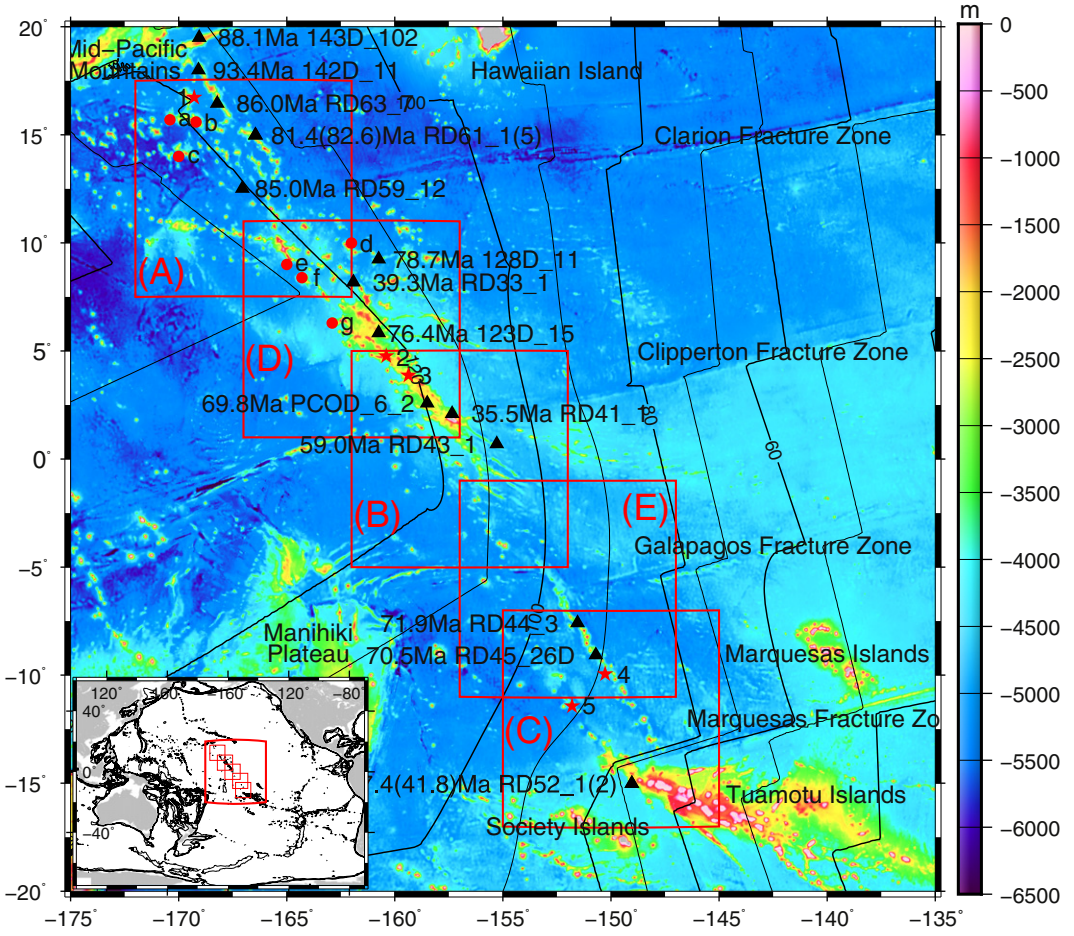

Fig. 1. A 1 × 1 minute bathymetry model created using ship soundings and vertical gravity gradient anomaly data (BAT_VGG) (Hu et al., 2014). Seafloor age data from Müller et al. (2008) are shown as contours (unit: Ma). The red boxes delineate the areas used to calculate the admittance curves in Fig. 4. Anotations: The red stars denote the islands of the Line Seamounts: 1 Johnston Atoll, 2 Washington Island, 3 Fanning Island, 4 Caroline Island, and 5 Flint Island. The red circles denote seamounts whose ages have been determined by Davis et al. (2002): a Keli Ridge West, b Keli Ridge East, c Smt.14 N 170 W, d Smt.10 N 162 W, e Smt.9 N 165 W, f S.P. Lee Guyot, and g Kingman Reef. The black triangles denote samples from Schlanger et al. (1984); the names and ages of the samples are given in the figure and details are provided in Table 3a, 3b.

supported by seafloor magnetism because most of the lithosphere under the Line ridge formed during the Cretaceous normal superchron (Atwater et al., 1993). Furthermore, the lithology of the Line ridge is similar to the Hawaiian-Emperor seamounts, and researchers have not found mid-ocean ridge basalt (Davis et al., 2002; Schlanger et al., 1984).

Despite the fact that the "hot spot" theory has been widely accepted, scholars note that "hot spots" are not the only tectonic activity that causes seafloor volcanism. Asthenospheric magma may erupt along fault zones and fracture zones caused by tensile forces. Natland (1976) argued that the generation of certain branches of the ridge may be associated with a rift in the seafloor. Lynch (1999) suggested that certain seamounts on the Pacific lithosphere may be related to tensional cracking based on the study of their geomorphology.

Based on the study of seamount ages and the lithology of the northern Line ridge, Davis et al. (2002) suggested that the formation of the Line ridge was influenced by Cretaceous super volcanic activity in the southern Pacific and argued that the multiple periods of volcanic activity along the ridge were caused by the eruption of mantle material in areas with weaker lithosphere. Zhang et al. (2006) studied the influences of fractures and Cretaceous magmatic activity on the construction of seamounts in the center of the Pacific. They suggested that fractures may weaken the local lithosphere, and magma may break through these weak zones.

To sum up: Volcanism along the Line ridge can't be explained by the hot spot theory. The morphology of the ridge may have been influenced by cracks of the lithosphere and fractures. However, these lithosphere-surface processes provide few explanations for magma generation. Ballmer et al. (2009) proposed an alternative mechanism to explain the non-hot spot intraplate volcanism. They argued that the small-scale sublithospheric convection (SSC) explains volcanism with no age progressions well. Volcanism over a "hot line" induced by SSC may continue for at least 10–20 Ma and occurs on seafloor ages of about 20–60 Ma. This mechanism reconciles quasi-synchronous eruption of seamounts over great distances along the Line ridge. Conrad et al. (2011) linked the intraplate volcanism to rapid asthenospheric shear. They find a correlation between recent intraplate volcanism and areas of the asthenosphere experiencing rapid shear by comparing the geographic distribution of intraplate volcanism with asthenospheric shear introduced by a global mantle flow model. They suggested that the driving mechanism for intraplate volcanism lies in the asthenosphere.

Because of its remote location, there have been few attempts to calculate the elastic thickness beneath the features of the Line ridge (Kalnins and Watts, 2009; Watts, et al., 2006). Kalnins and Watts (2009) introduced the moving window admittance technique (MWAT) to determine the spatial variation of *Te* in the Western Pacific, based on GEBCO_08 (General Bathymetric Charts of the Oceans) and

altimetric gravity anomaly data from Scripps Institute of Oceanography (SIO, V16.1). *Te* is estimated via 3D spectral analysis for different window sizes (400 × 400 km to 1400 × 1400 km). The final *Te* is computed from the weighted average of the results for different window sizes.

Hu et al. (2014) constructed a new bathymetry model (BAT_VGG), by combining vertical gravity gradient anomalies and ship soundings. In this study, we re-calculate *Te* of the Line ridge using the MWAT introduced by Kalnins and Watts (2009) and the BAT_VGG. The correlation between *Te* and the age of the lithosphere at the time of loading is evaluated based on our estimates.

2. Theory and method

2.1. The lithospheric flexural isostatic model

The theoretical basis for *Te* estimation is the flexural isostatic model (Watts, 2001). Fig. 2 illustrates a simple flexural crustal model, in which $h(x)$ is the seafloor topography and $r(x)$ is the flexure of the Moho discontinuity introduced by the topographic loading. The parameters of this simple model are summarized in Table 1.

In the frequency domain, the theoretical admittance according to the flexural isostatic model given by Watts (2001) is as follows:

$$Z(k) = 2\pi G(\rho_c - \rho_w)e^{-kd}\left(1 - \Phi_e(k)e^{-kt}\right) \quad (1)$$

where G is the universal gravitational constant, d is the mean water depth, t is the mean crustal thickness, $k = 2\pi/\lambda$ is the wave number, λ is the wavelength; ρ_m, ρ_c, and ρ_w are the density of the mantle, crust, and seawater, respectively; and $\Phi_e(k)$ is the flexural response function of the lithosphere, as given by (Walcott, 1970):

$$\Phi_e(k) = \left[\frac{Dk^4}{(\rho_m - \rho_c)g} + 1\right]^{-1} \quad (2)$$

where g is the average gravitational acceleration, D is the flexural rigidity of the lithosphere, and $D = ET_e^3/[12(1-\upsilon^2)]$, E is Young's modulus, and υ is Poisson's ratio. The theoretical admittance curves for different parameter values are shown in Fig. 3.

According to Fig. 3(a), at wavelengths shorter than 50 km, the theoretical admittance does not change significantly for different *Te* values because the topography is uncompensated at these wavelengths. This provides us with a chance to recover crustal density based on admittance fitting at 20–50 km wave bands. The uncompensated theoretical admittance $Z_{uncom}(k)$, the thick blue line in Fig. 3(a), is given by:

$$Z_{uncom}(k) = 2\pi G(\rho_c - \rho_w)e^{-kd}. \quad (3)$$

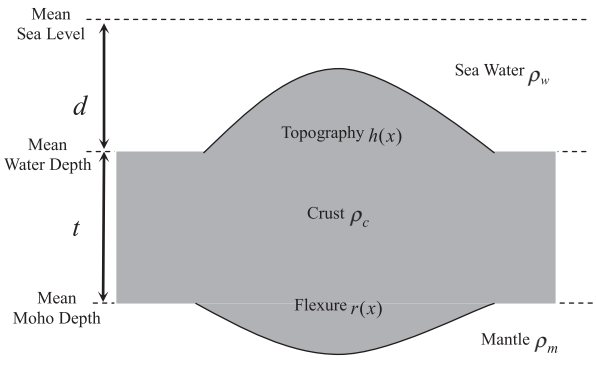

Fig. 2. The simple flexural isostatic model.

Table 1
Summary of parameters assumed for the simple flexural isostatic model.

Parameter	Notation in equations	Value
Density of seawater	ρ_w	1030 kg/m^3
Density of crust	ρ_c	2800 kg/m^3
Density of mantle	ρ_m	3350 kg/m^3
Mean crustal thickness	t	6.5 km
Young's modulus	E	10^{11} N/m^2
Poisson's ratio	υ	0.25

2.2. 3D spectral analysis of Te

Te can be estimated using the 3D spectral analysis method, by fitting the observed and theoretical admittance. The theoretical admittance can be calculated with Eq. (1). The observed admittance, $Z'(k)$, can be determined with the observed gravity anomaly data, $\Delta G'(k)$, and the

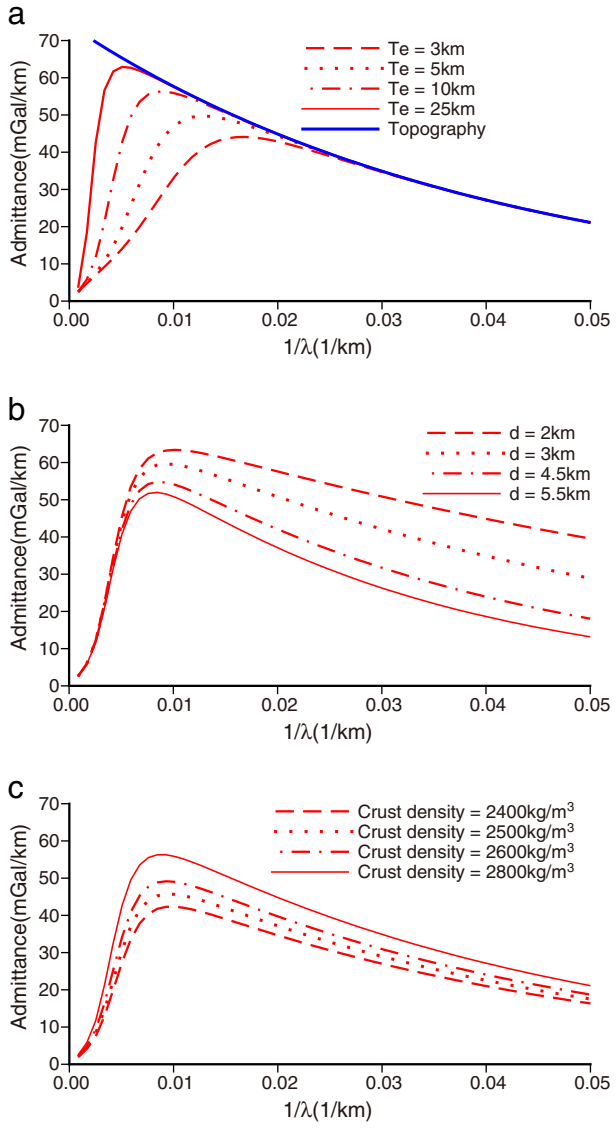

Fig. 3. The theoretical admittance curves for different flexural models. (a) Admittance for a fixed d (4 km), ρ_c(2800 kg/m^3), and T_e in the range of 3–25 km. The thick blue line denotes the uncompensated admittance between the bathymetry and the gravity anomaly. (b) Admittance for a fixed T_e (10 km), ρ_c(2800 kg/m^3), and d in the range of 2–5.5 km. (c) Admittance for a fixed T_e (10 km), d (4 km), and ρ_c in the range of 2400–2800 kg/m^3.

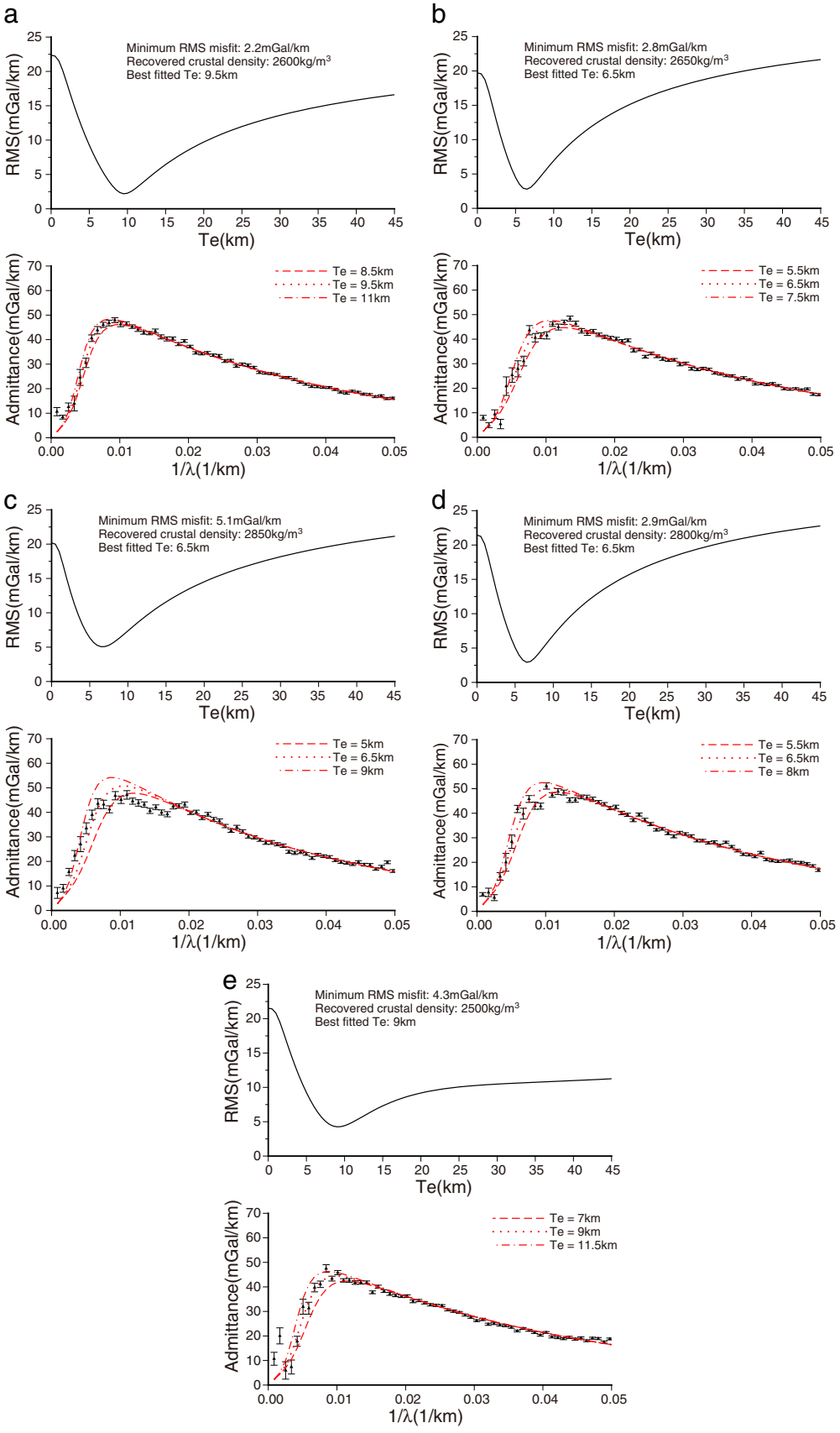

Fig. 4. Fit of observed (black triangles) and theoretical (red dotted, dashed, and dot-dashed lines) admittance curves for the five experimental areas in Fig. 3. RMS misfits are provided for different *Te* values (up) and the best fitted T_e are shown (down).

seafloor topography model, $B(k)$, using the following equation (McNutt and Judge, 1990):

$$Z'(k) = \frac{<G'(k) \cdot B^*(k)>}{<B(k) \cdot B^*(k)>} \quad (4)$$

where * denotes the complex conjugate and < > indicates annular averaging of the spectral estimates.

Te can be established by minimizing the RMS misfit between the observed and theoretical admittance. The technique is put forward as a two-step procedure. First, at the 20–50 km wave bands, the uncompensated theoretical admittance is calculated using Eq. (3) for different ρ_c (2300–2900 kg/cm^3) and d (mean model depth ± 500 m). The value of ρ_c and d can be recovered for each area by fitting the theoretical and observed admittance. Second, at wave lengths longer than 50 km, with the recovered ρ_c and d, the theoretical admittance can be computed using Eq. (1) for different *Te*. We obtain an optimal *Te* when the RMS misfit is minimized.

The five experimental areas A–E (centered on, A: 193°E,12.5°N, B: 203°E,0°, C: 210°E,12°S, D: 198°E, 6°N, E: 208°E, 6°S) are shown in Fig. 1. The fits between the observed and theoretical admittances for a 10° × 10° window in each area are shown in Fig. 4. The calculated *Te* represents the regional strength of the lithosphere under each area. The gravity and bathymetry grids used are SIO V20.1 (Sandwell and Smith, 2009) and BAT_VGG.

According to Fig. 4, the physically plausible values of the crustal density can be recovered, and the *Te* estimates of the five sample areas (A–E) are 9.5 km, 6.5 km, 6.5 km, 6.5 km, and 9 km, respectively. The minimum RMS misfits between the observed and theoretical admittance curves for the five areas are 2.2 mGal/km, 2.8 mGal/km, 5.1 mGal/km, 2.9 mGal/km, and 4.3 mGal/km, respectively. The *Te* estimated by MWAT represents the mean strength of the lithosphere for the area covered by the input data.

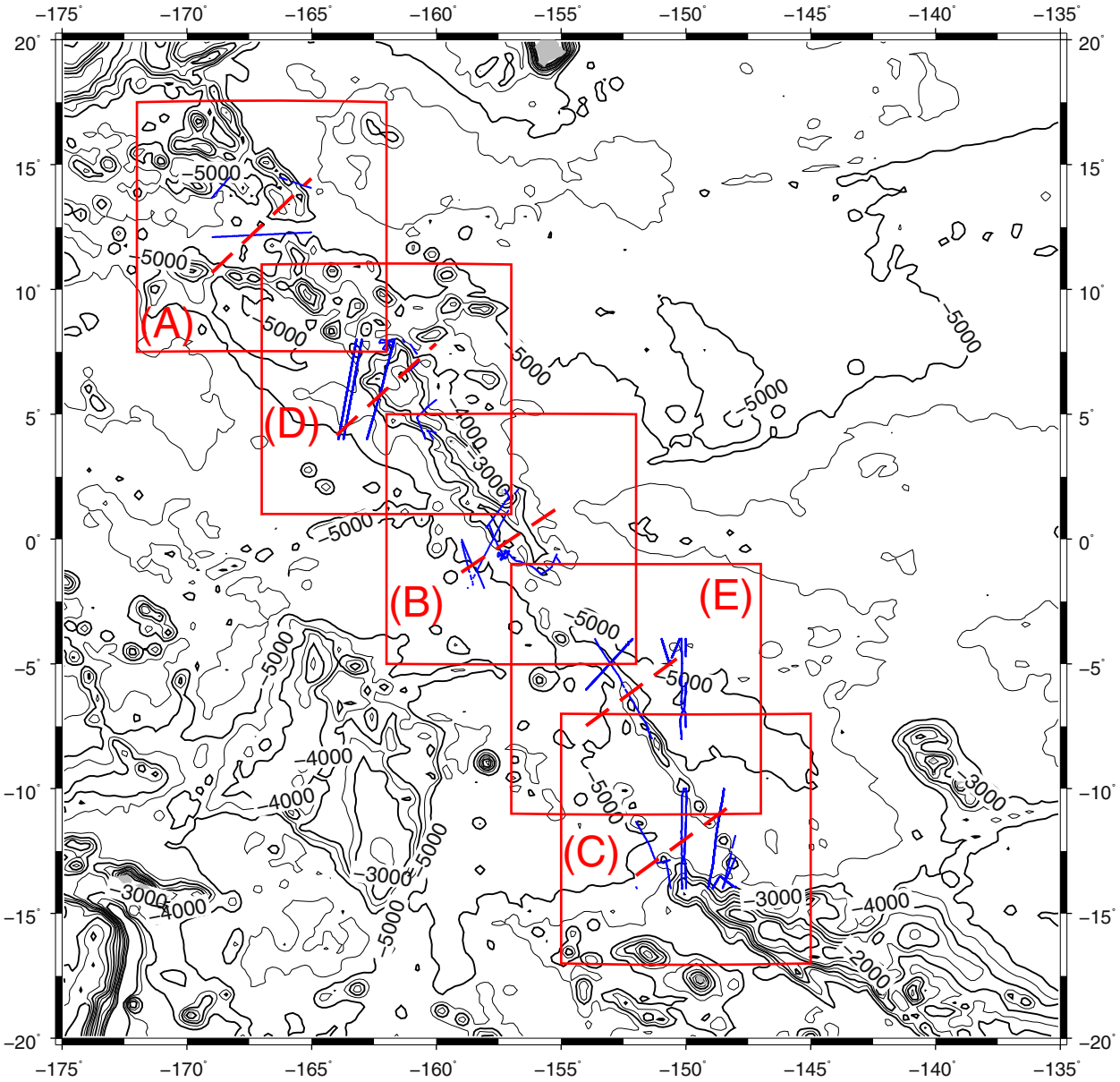

Fig. 5. Distribution of shipborne gravity (the blue line) and altimetric gravity profiles from SIO V20.1 (the red-dashed line), contours are bathymetry from BAT_VGG (unit: m).

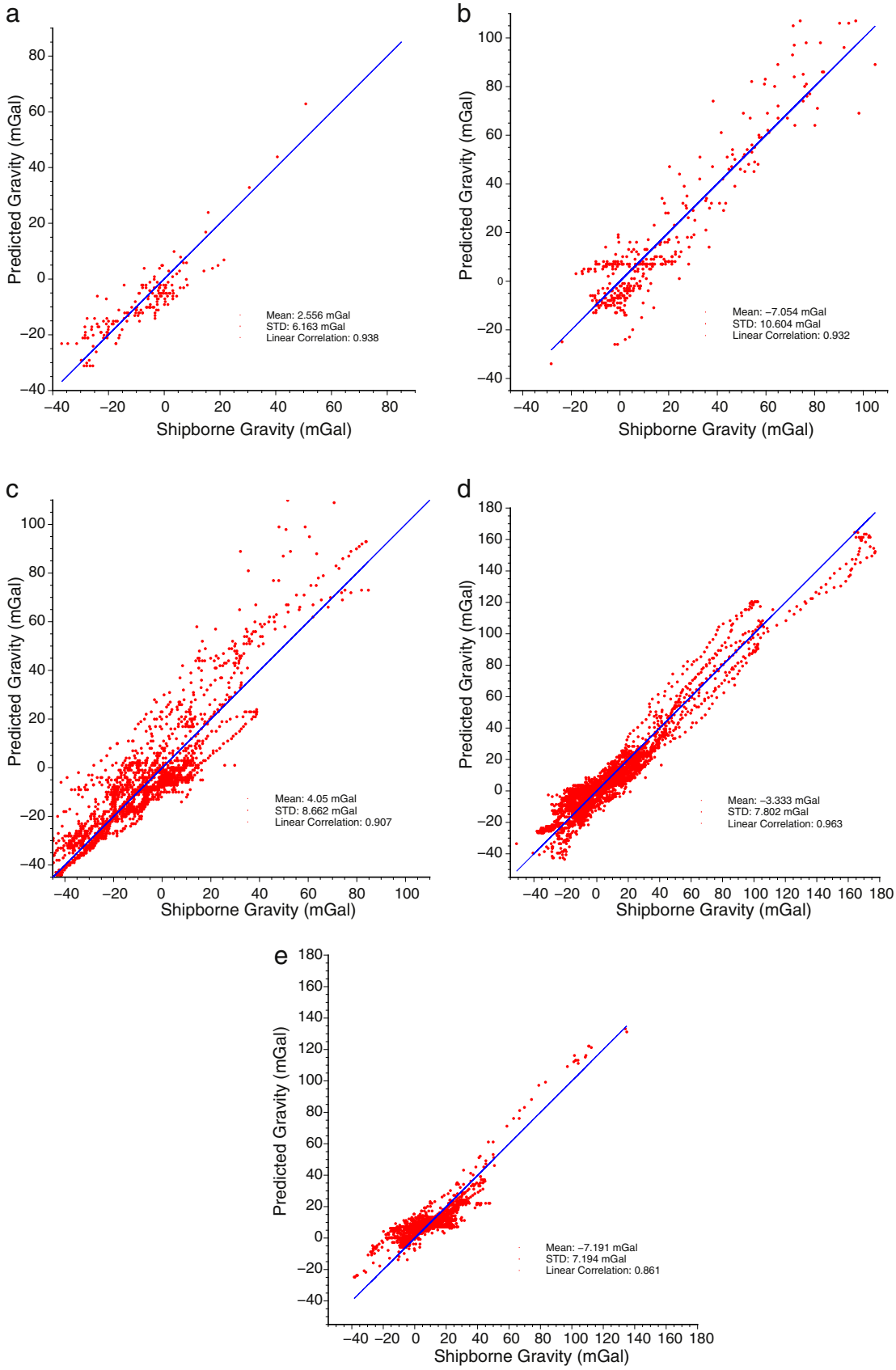

Fig. 6. Comparison of shipborne and predicted gravity in regions A–E. The shipborne gravity data is downloaded from NGDC and the predicted gravity are calculated using T_e and crustal parameters from Fig. 4 and the BAT_VGG grid.

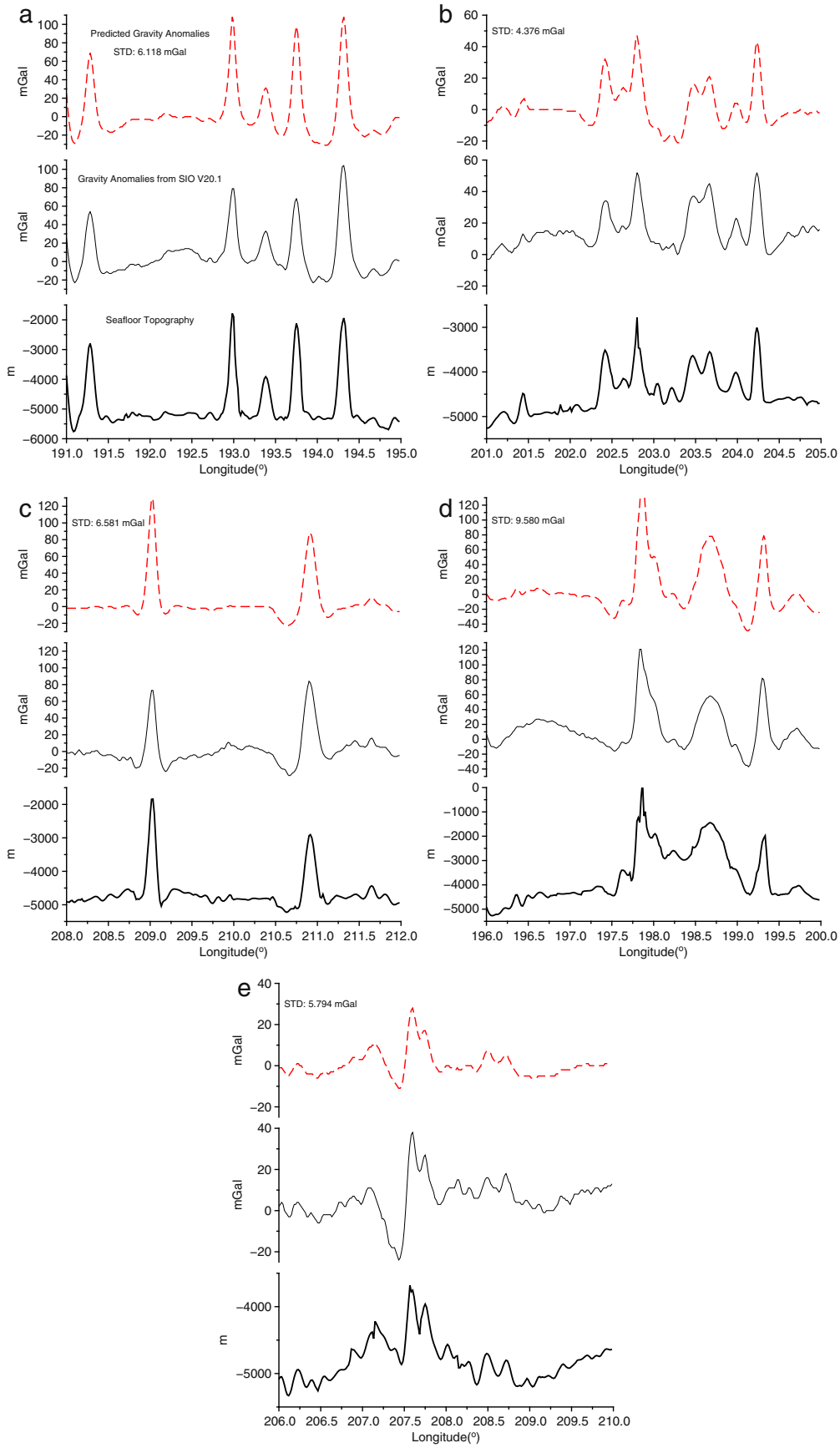

Fig. 7. Comparison of predicted gravity and altimetric gravity (SIO V20.1) for the five profiles. The thick-black lines denote seafloor topography profiles from BAT_VGG. The thin-black lines give altimetric gravity from SIO V20.1. The red-dashed lines show predicted gravity, which were calculated based on the T_e and crustal parameters from Fig. 4 and the BAT_VGG grid. The standard deviations (STD) between predicted and altimetric gravity of all the five profiles are also given in the figures.

2.3. Validation

We validated the results in samples A–E using shipborne gravity and altimetric derived gravity (SIO V20.1). This is a poorly-surveyed area, but we obtained a few shipborne gravity data from NGDC (National Geophysical Data Center, US). Fig. 5 (the blue lines) shows the distribution of shipborne gravity at the center of a 4° × 4° area for each region. The shipborne gravity was evaluated using the altimetric gravity (SIO V20.1), and tracks with obvious errors were deleted. The deleted data accounts for less than 1% of the total shipborne data. The red-dashed lines are gravity profiles perpendicular to the ridge.

The *Te* and crustal parameters for areas A–E and the BAT_VGG grid were used to predict gravity anomalies on the sea surface. Fig. 6 shows the comparison between predicted and shipborne gravity anomalies. There are always high linear correlations between them.

Fig. 7 shows five profiles perpendicular to the ridge. The lower thick line gives seafloor topography from BAT_VGG. The middle thin line gives altimetric gravity from SIO V20.1. The upper red-dashed line gives predicted gravity. The standard deviations between SIO V20.1 and predicted gravity of the five profiles are also given. These results indicate that a geophysically reasonable *Te* can be recovered using the BAT_VGG grid and the 3D spectral analysis method.

3. Data and results

3.1. Data

In this study, we use gravity anomaly data from SIO (Version V20.1), which are derived from satellite altimetric observations (Sandwell and Smith, 2009). For comparison, three types of bathymetry models, GEBCO_08, SIO V15.1, and BAT_VGG are used to calculate T_e. GEBCO_08 is a 1-minute grid prepared from bathymetric contours of the world's oceans and soundings, with interpolation between soundings guided by satellite-derived gravity data. SIO V15.1 was released by the Scripps Institute of Oceanography (SIO), UCSD, and was derived from ship soundings and satellite altimetric gravity anomalies (Smith and Sandwell, 1997). BAT_VGG was created using ship soundings and vertical gravity gradient anomalies (Hu et al., 2014). In the northwest Pacific (145°–215°E, −15°–45°N), the accuracies of these models are assessed with ship soundings and are shown in Table 2. The frequency distribution histogram of water depths in the northwest Pacific is shown in Fig. 8.

According to Table 2, the accuracy of GEBCO_08 is significantly lower than that of SIO V15.1 and BAT_VGG. The BAT_VGG model is used in this problem for the first time.

Fig. 8 shows that GEBCO_08 still has the statistical bias problem of "terrace" (Smith, 1993), due to this bathymetry grid's strong dependence on contours.

3.2. Results

In our study, 1° × 1° *Te* grids were calculated for the Line ridge and its adjacent areas (185°–225°E, −20°–20°N), with 1681 nodes calculated in all. The statistics of the recovered crustal densities and minimal RMS misfits are given in Table 3a. The statistics of the northwest Pacific (145°–215°E, −15°–45°N) are also given in Table 3b.

Table 2
Differences between the bathymetry models and ship soundings (unit: m).

Model name	Min	Max	Mean	STD
GEBCO	−1264.908	1265.306	15.845	291.427
SIO V15.1	−305.377	305.352	−2.880	57.692
BAT_VGG	−462.542	462.551	6.239	95.049

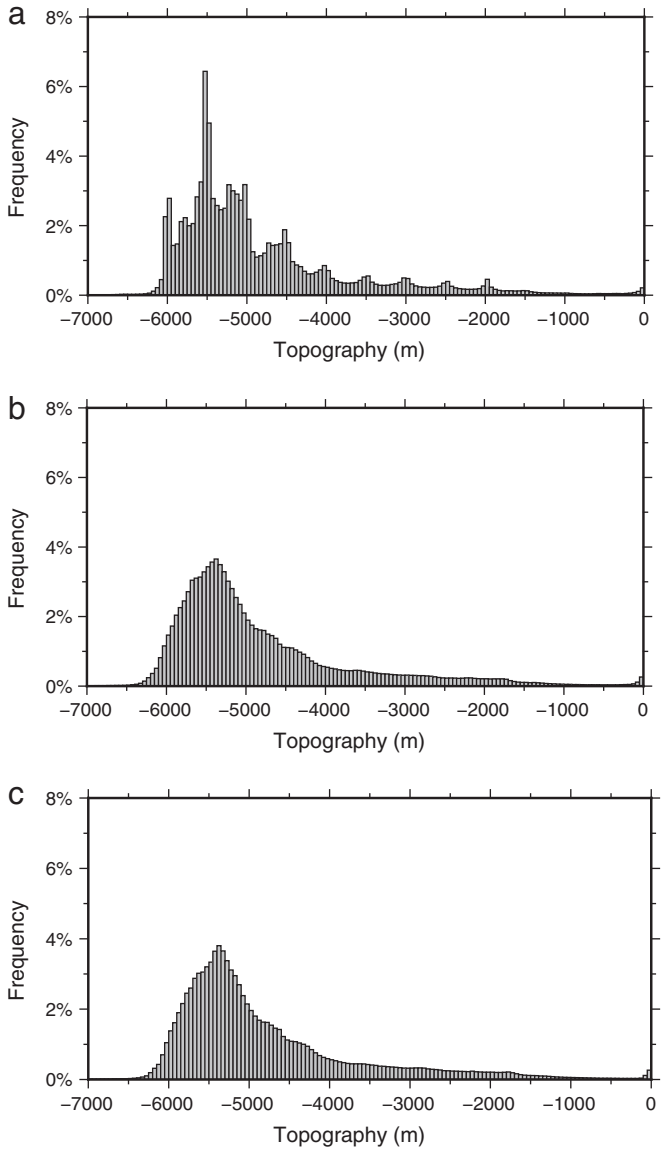

Fig. 8. Frequency distribution of seafloor topography in the northwest Pacific (a for GEBCO_08, b for SIO V15.1, and c for BAT_VGG).

According to Tables 3a, 3b, when using BAT_VGG to estimate T_e, the geophysically reasonable crustal density can be recovered, which is consistent with the mean crustal density given by CRUST2.0 (2757 kg/m^3 in the Line ridge and its adjacent areas, and 2772 kg/m^3 in the northwest Pacific). Nearly all of the minimal RMS misfits between the observed and theoretical admittance are less than 10 mGal/km. These results confirm that the BAT_VGG model is suitable for estimating *Te*, while SIO V15.1 can also be used. In fact, Smith and Sandwell (1994) designed special filters to shape the inverse transfer function, and the altimetric gravity anomalies are used to predict bathymetry in the waveband range of 15–160 km. Thus, SIO V15.1 is only weakly dependent on T_e. *Te* of the Line ridge calculated with BAT_VGG is discussed in this paper.

The distributions of the RMS misfits and *Te* values for the study area are shown in Figs. 9 and 10, respectively. In the study area, the mean and STD of the *Te* are 11.9 km and 7.5 km, respectively. For the Line ridge, the *Te* is approximately 5.5–13 km.

According to Fig. 9, the theoretical admittance fits the observed admittance well, and the RMS misfits are less than 5 mGal/km along the ridge.

Table 3a
Recovered mean oceanic crust density and RMS of the differences between theoretical and measured admittance when using different bathymetry models (for the Line ridge and its adjacent areas).

Bathymetry model	The mean (STD) of recovered crustal density (kg/m^3)	The mean (STD) of RMS misfit between observed and theoretical admittance (mGal/km)	The percentage of grid nodes with RMS ≤ 5 mGal/km	The percentage of grid nodes with RMS ≤ 10 mGal/km
GEBCO_08	2467(±192)	7.5(±2.5)	13.9%	86.1%
SIO V15.1	2696(±104)	5.4(±1.8)	44.1%	99.7%
BAT_VGG	2733(±125)	4.8(±2.2)	65.2%	97.6%

Table 3b
Recovered mean oceanic crust density and RMS of the differences between theoretical and measured admittance when using different bathymetry models (for the northwest Pacific).

Bathymetry model	The mean (STD) of recovered crustal density (kg/m^3)	The mean (STD) of RMS misfit between observed and theoretical admittance (mGal/km)	The percentage of grid nodes with RMS ≤ 5 mGal/km	The percentage of grid nodes with RMS ≤ 10 mGal/km
GEBCO_08	2562(±211)	7.5(±2.6)	11.8%	85.5%
SIO V15.1	2720(±148)	5.6(±2.2)	46.2%	95.4%
BAT_VGG	2770(±120)	5.2(±2.5)	56.9%	95.5%

Fig. 10 shows that the T_e along the ridge is not changing progressively, but instead exhibits segmentations. The strength of the lithosphere under region A and E is higher than that of other areas slightly. Most of the T_e estimates in region A and E are 8–12 km, and so these seamounts are "flank ridge" features, according to Watts et al. (2006). The continuity of the Line and Caroline Islands is interrupted in region E. The lithosphere under the Line Islands (regions B and D) is weaker, and show lower T_e of 4–8 km. This means that the Line Islands are an "on ridge" setting. The upper-right corner of Fig. 10 shows the T_e of the Hawaiian-Emperor chain. As a chain constructed by a "hot spot", the T_e decreases gradually from southeast to northwest, with increasing distance from the hot spot. This indicates that the Line ridge may have been modified by tectonic activities more complicated than those of a "hot spot".

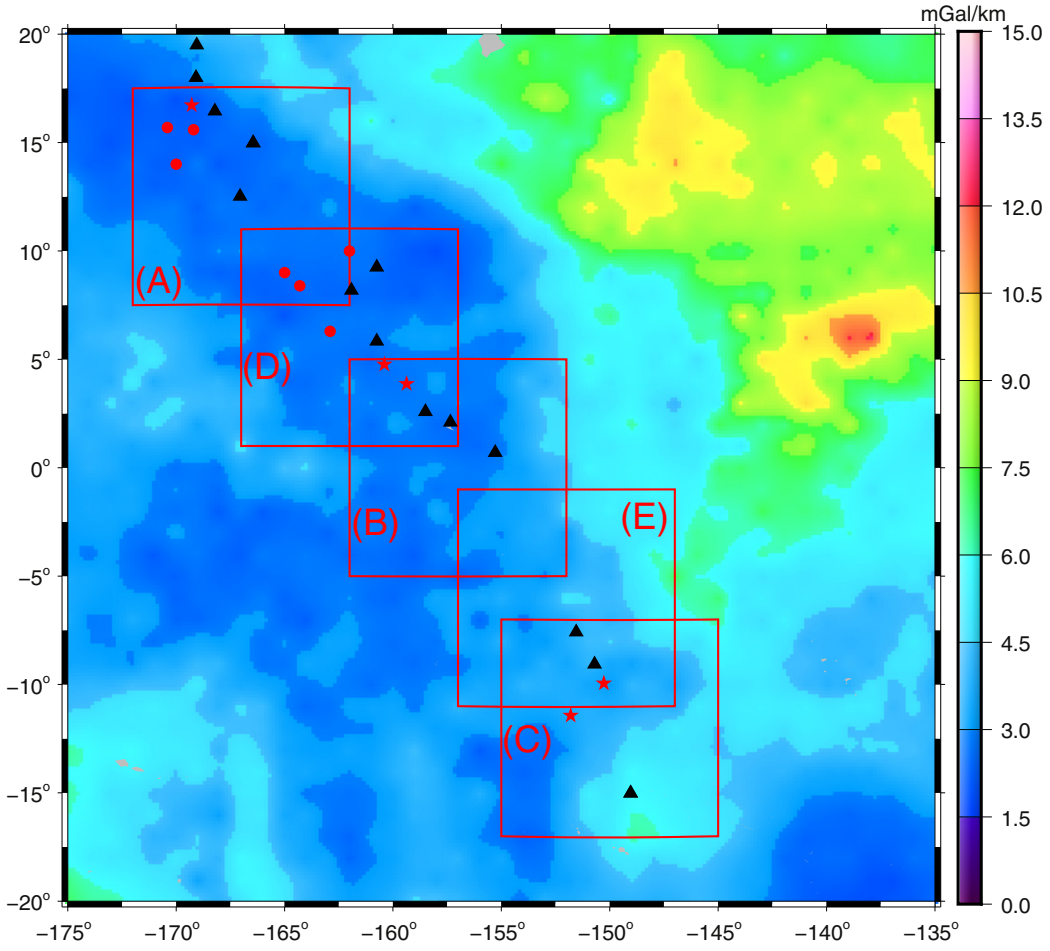

Fig. 9. Minimum RMS misfits between measured and theoretical admittances.

Watts et al. (2006) calculated the *Te* of the lithosphere under more than 9000 seamounts using the bathymetry prediction method and seamount database provided by Wessel (2001). In the study area of this paper, the *Te* values of approximately 543 seamounts are calculated. Fig. 11(a) shows the results given by Watts et al. (2006). The *Te* of the Line ridge shows a similar trend with our results, except for a few values greater than 20 km. Fig. 11(b) shows the differences between our results and those of Watts et al. (2006). Most of the absolute differences are less than 5 km.

Both the MWAT and the bathymetry prediction method have advantages and disadvantages when estimating T_e. The MWAT takes into account both the near and far zone loads but reduces the resolution. The bathymetry prediction method can be used easily to calculate *Te* under an individual seamount, but it may overestimate *Te* if adjacent loads are ignored (Kalnins and Watts, 2009), especially for a smooth basin. The method of Watts et al. (2006) is generally applied to an isolated seamount that has been surveyed by ship soundings, while the MWAT can be used to estimate the *Te* for nearly the entirety of the seafloor.

4. Discussions and conclusions

The relationship between *Te* and the age of the lithosphere at the time of loading is analyzed here. Ages of 21 seamounts were collected from Schlanger et al. (1984) and Davis et al. (2002) (Table 4). There is no clear hot-spot age progression along the ridge. Table 4 also lists the seafloor age at the time of loading and the *Te* values calculated in this paper.

The relationship between *Te* and the age of the seafloor at the time of loading is shown in Fig. 12.

Both the *Te* samples of the Line ridge and the Hawaiian-Emperor seamounts are shown in Fig. 12 for comparison. According to Fig. 12, most of the *Te* along the Hawaiian-Emperor seamounts are located at the 300–450 °C isotherm depth, while most of the T_e along the Line ridge are located at the 150–300 °C isotherm depth. Kalnins and Watts (2009) show that *Te* of the Cretaceous lithosphere for the northwestern Pacific is in the 180 ± 120 °C isotherm depth range, and the results in this paper agree with this finding. Based on the data along the Line ridge in Table 4, the age of the seafloor at the time of loading can be divided into two parts. Some of the seamounts have ages older than 80 Ma and formed on 20–35 Ma seafloor, and the other seamounts have ages that are approximately 70 Ma and developed when the seafloor age was approximately 40–60 Ma. As shown in Table 4 and Fig. 12, the *Te* of these seamounts are similar. These results may suggest that the lithosphere of the Line ridge, as a whole, experienced certain geologic processes, such as thermal activation, fracture, etc., which weakened its strength.

The origin of the Line ridge can be discussed based on *Te* of the lithosphere. The *Te* is the product of a combination of various tectonic forces experienced by the lithosphere. The tectonic origin of the seamount chain can be discussed based on *Te*, seamount ages, bathymetry, and lithology.

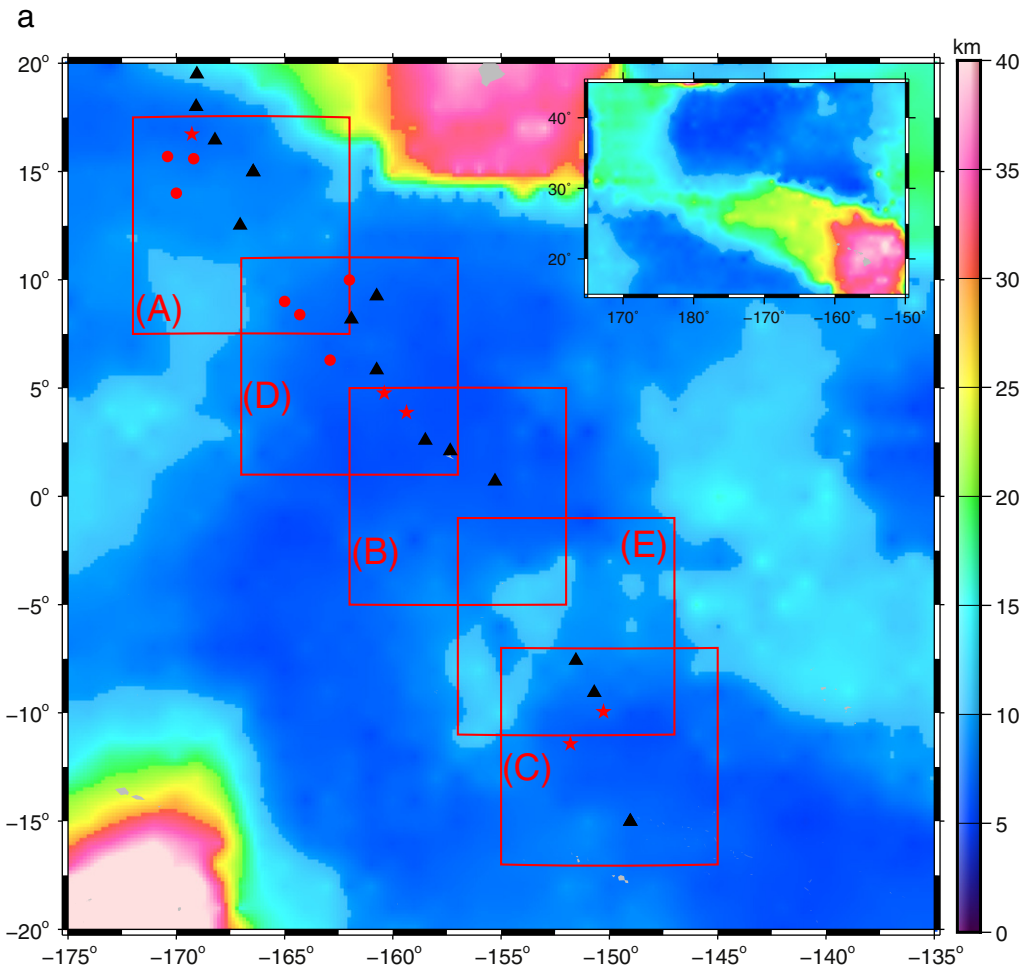

Fig. 10. *Te* of the lithosphere under the Line ridge and its adjacent areas (a) and the frequency distribution of *Te* in the five experimental regions. (*Te* of the Hawaiian-Emperor chain are shown at the upper-right corner for comparison).

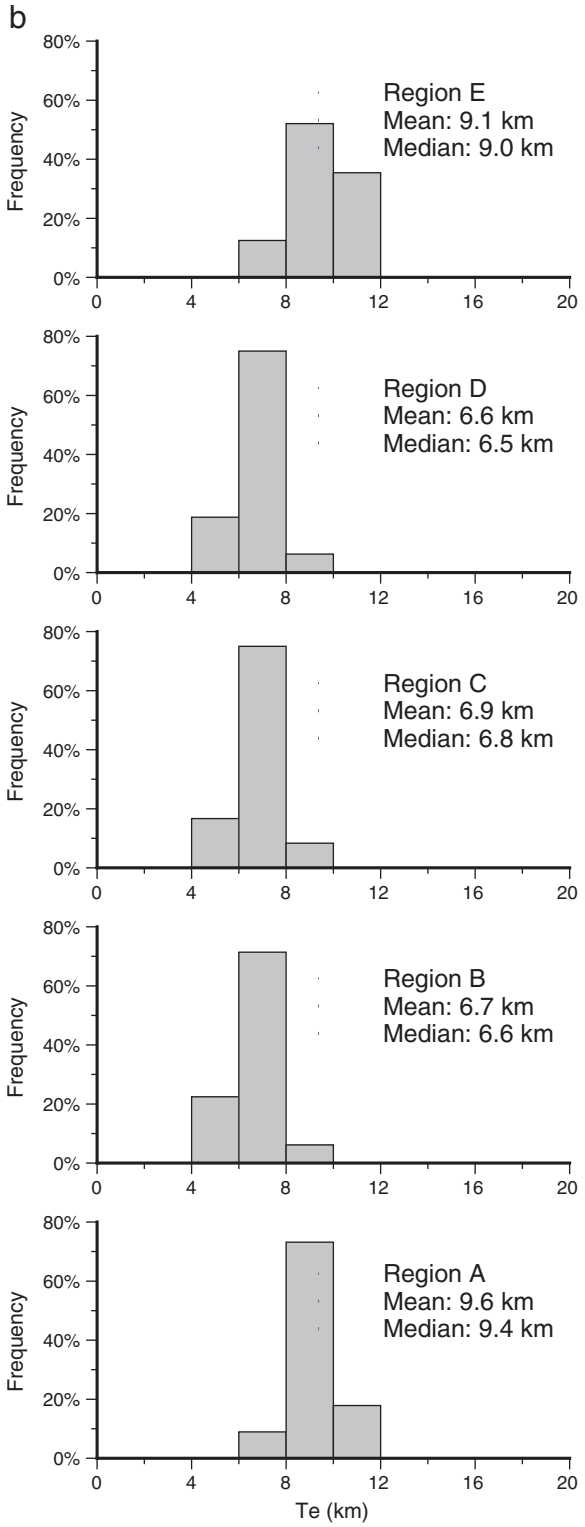

Fig. 10 (*continued*).

The *Te* structure of the Line ridge may be related to special tectonic activity. At about 80 Ma, the first phase of the ridge formed in association with the Cretaceous super volcanic activity in the south Pacific when the lithosphere age was approximately 20–35 Ma. As the plate drifted north, magma erupted again along a weak part of the lithosphere when the lithosphere age was approximately 40–60 Ma. At approximately 43 Ma, the drift direction of the Pacific Plate changed, and this may have changed the stress field of the plate and led to the last stage of volcanism of the Line ridge, especially in the area of the Line Islands (Sager and Keating, 1984). The existence of thermal activity, fracture zones, and changes in stress may all have weakened the lithosphere.

There is no progression in seamount ages and T_e along the Line ridge. The present analysis leads us to the following conclusions:

(1) When we estimated *Te* using BAT_VGG, the geophysically reasonable crustal density was recovered, which is consistent with the density from CRUST2.0. Most of the RMS misfits between the observed and theoretical admittance results are less than 5 mGal/km. These results indicate that BAT_VGG is suitable to calculate *Te*.

(2) The *Te* along the Line ridge is approximately 5.5–13 km, with a mean of 8 km and a standard deviation of 1.3 km. The *Te* of the Line ridge exhibits no trend, unlike the Hawaiian-Emperor chain, but instead exhibits segmentation. The structure of the Line and Caroline Islands is discontinuous from the perspective of *Te* (interrupted at region E). Thus, region E experienced weaker thermal activity than region B and D, and shows less volcanism.

(3) Most of the *Te* values for the Line ridge are located at the 150–300 °C isotherm depth, which is significantly less than the depth given by Watts (2001), which is 300–600 °C. The age of the lithosphere at the time of seamount loading appears to be concentrated in two periods: 20–35 Ma and 40–60 Ma. Despite the age differences, this study found similar *Te* for the lithosphere of these age groups. Our findings may indicate that the lithospheric strength was weakened by geologic processes. Thus, the strength of the lithosphere under the Line ridge is not solely controlled by the age of the lithosphere at the time of loading, but the thermal and fracture activities must have played an important role in the origin and evolution of the ridge. Due to the extended distribution of seamounts and the volcano ages along the Line Islands, these thermal activities may be attributed to the small-scale sublithospheric convection (SSC) (Ballmer et al., 2009). Volcanism continued for about 60 Ma on the seafloor with ages larger than 100 Ma now, as showed in Table 4. This can be explained by the SSC model with high reference mantle temperature. While, it is reasonable to suppose that the mantle temperature under the Line ridge is higher than normal for the ridge is constructed near the south Pacific “super swell”.

Acknowledgments

The study was supported financially by the Key Foundation of the Institute of Seismology, China Earthquake Administration (IS201506205), and the Industry Research of China Earthquake Administration (201508006). We thank the anonymous reviewers for their comments that greatly helped to improve this paper.

References

Atwater, T., Schlater, J., Sandwell, D., Severinghaus, J., & Marlow, M.S., 1993. Fracture zone traces across the north Pacific cretaceous quiet zone and their tectonic implications. In: Pringle, M.S., Sager, W.W., Sliter, W.V., Stein, S. (Eds.), The Mesozoic Pacific: Geology, Tectonics and VolcanismGeophys. Monograph Ser. vol. 77. AGU, Washington, D.C., pp. 137–154. http://dx.doi.org/10.1029/GM077p0137.

Ballmer, M.D., Hunen, J., Ito, G., Bianco, T.A., & Tackley, P.J., 2009. Intraplate volcanism with complex age–distance patterns: a case for small-scale sublithospheric convection. Geochem. Geophys. Geosyst. 10, Q06015. http://dx.doi.org/10.1029/2009GC002386.

Calmant, S., Francheteau, J., & Cazenave, A., 1990. Elastic layer thickening with age of the oceanic lithosphere: a tool for prediction of the age of volcanoes or oceanic crust. Geophys. J. 100, 59–67. http://dx.doi.org/10.1111/j.1365-246X.1990.tb04567.x.

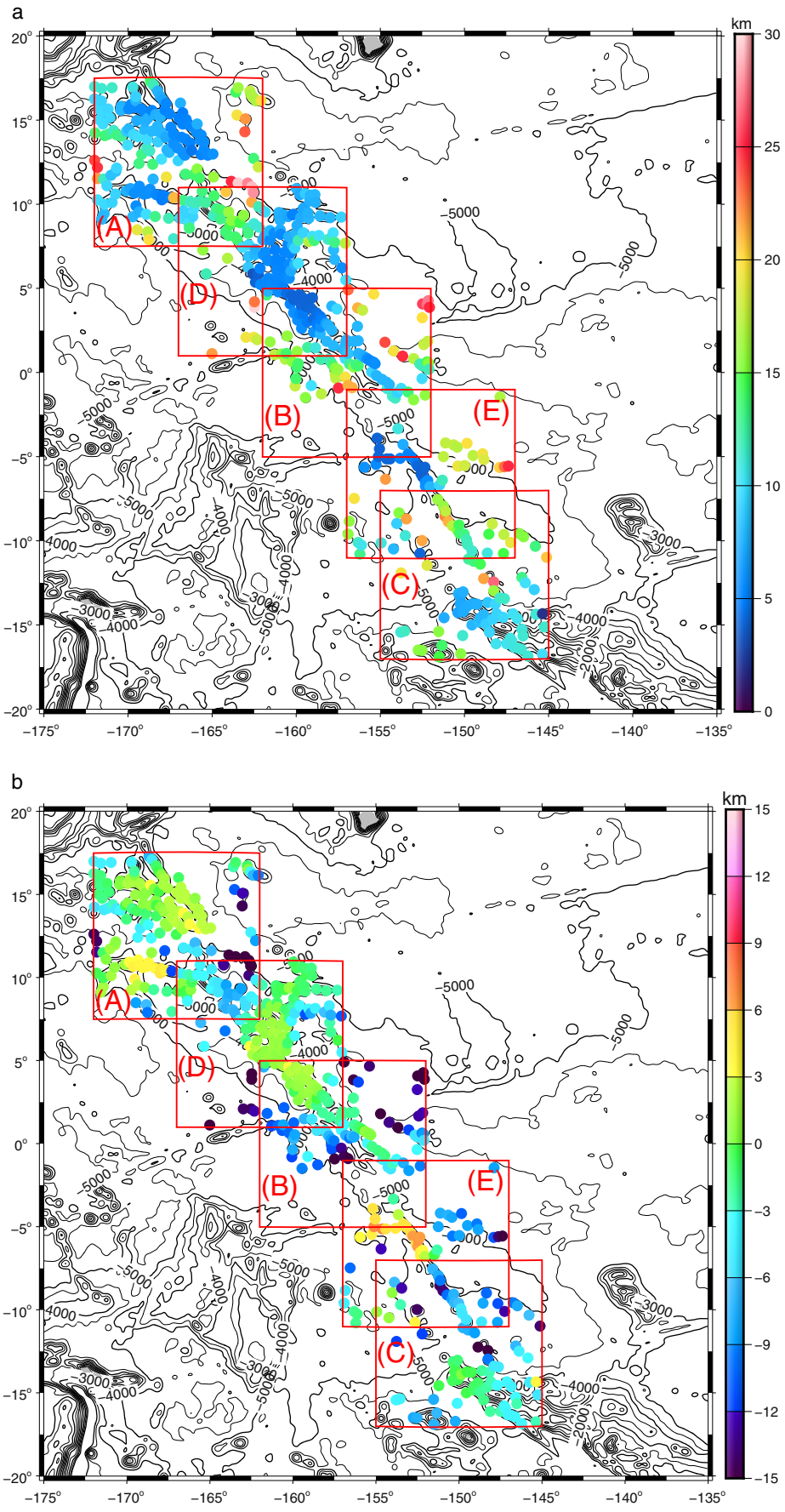

Fig. 11. Lithospheric effective elastic thickness under certain seamounts of the Line ridge given by Watts et al. (2006)(a); and differences between results calculated in this study and that of Watts et al. (2006) (b); (Background contours are based on bathymetry model BAT_VGG).

Table 4
Seamount ages and *Te* of the Line ridge.

Samples' name	Location	Age of seafloor (Ma)	Age of seamount (Ma)	Age of seafloor at time of loading (Ma)	*Te* (km)
143D_102	169°03′W,19°30′N	110.8	88.1	22.7	13.2
142D_11	169°05′W,18°00′N	114.2	93.4	20.8	10.8
RD63_7	168°13′W,16°27′N	115.3	86.0	29.3	8.2
RD59_12	167°03′W,12°31′N	120.6	85.0	35.6	8.7
RD61_1(5)	166°27′W,14°59′N	113.8	82.0	31.8	8.9
128D_11	160°45′W,09°15′N	112.8	78.7	34.1	7.3
RD33_1	161°55′W,08°11′N	118.6	39.3	79.3	7.2
123D_15	160°45′W,05°50′N	122.4	76.4	46.0	6.5
PCOD_6_2	158°30′W,02°35′N	119.5	69.8	49.7	6.0
RD41_1	157°21′W,02°06′N	115.1	35.5	79.6	5.6
RD43_1	155°17′W,00°42′S	108.0	59.0	49.0	6.9
RD44_3	151°33′W,07°35′S	93.7	71.9	21.8	8.7
RD45_26D	150°42′W,09°04′S	90.7	70.5	20.2	7.4
RD52_1(2)	149°02′W,15°01′S	66.9	44.6	22.3	8.2
Johnston Atoll	169°17′W,16°44′N	118.9	71.2	47.7	7.7
Keli Ridge West	170°24′W,15°42′N	121.5	70.8	50.7	8.6
Keli Ridge East	169°12′W,15°36′N	119.3	67.6	51.7	7.7
Smt.14N170W	170°00′W,14°00′N	125.6	68.1	57.5	8.1
Smt.10N162W	162°00′W,10°00′N	114.7	83.6	31.1	7.7
Smt.9N165W	165°00′W,09°00′N	125.6	69.3	56.3	8.5
Kingman Reef	162°54′W,06°18′N	125.3	70.0	55.3	7.2

Annotations: The sample names, locations, and ages are from Schlanger et al. (1984) and Davis et al. (2002). The age of the seafloor is interpolated from Müller et al. (2008). The age of the seafloor at the time of loading is defined as the age difference between the seafloor and the seamounts. *Te* is calculated by MWAT using the bathymetry model BAT_VGG and altimetric gravity anomalies SIO V20.1.

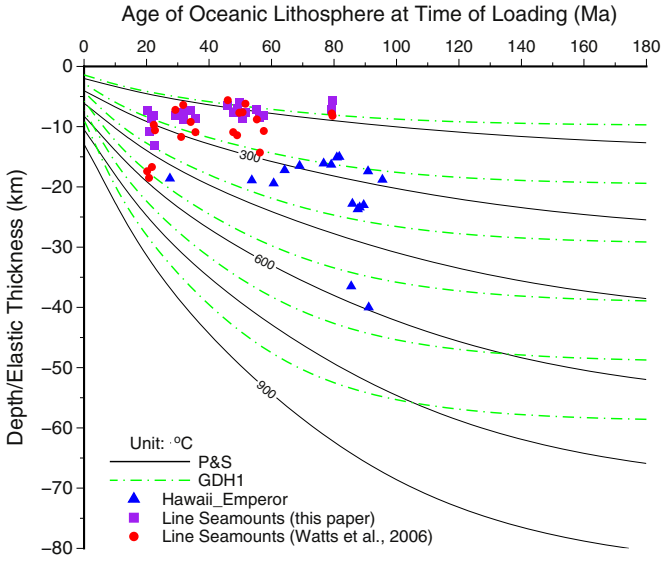

Fig. 12. Relationship between the effective elastic thickness and the age of the oceanic lithosphere at the time of loading. (P&S: model given by Parsons and Sclater (1977); GDH1: model given by Stein and Stein (1992). Purple squares represent the results from this paper, red circles represent results from Watts et al. (2006), and blue triangles represent the results for the Hawaiian-Emperor seamounts).

Conrad, C.P., Bianco, T.A., Smith, E.I., & Wessel, P., 2011. Patterns of intraplate volcanism controlled by asthenospheric shear. Nat. Geosci. 4, 317–321. http://dx.doi.org/10.1038/NGEO1111.

Davis, A.S., Gray, L.B., Clague, D.A., & Hein, J.R., 2002. The Line Islands revisited: New $^{40}Ar/^{39}Ar$ geochronologic evidence for episodes of volcanism due to lithospheric extension. Geochem. Geophys. Geosyst. 3. http://dx.doi.org/10.1029/2001GC000190.

Hu, M., Li, J., Li, H., Shen, C., Jin, T., & Xing, L., 2014. Predicting global seafloor topography using multi-source data. Mar. Geod. http://dx.doi.org/10.1080/01490419.2014.934415.

Kalnins, L.M., & Watts, A.B., 2009. Spatial variations in effective elastic thickness in the western Pacific ocean and their implications for Mesozoic volcanism. Earth Planet. Sci. Lett. 286, 89–100. http://dx.doi.org/10.1016/j.epsl.2009.06.018.

Lynch, M.A., 1999. Linear ridge groups: evidence for tensional cracking in the Pacific plate. J. Geophys. Res. 104 (B12), 29321–29333. http://dx.doi.org/10.1029/1999JB900241.

McNutt, M.K., & Judge, A.V., 1990. The superswell and mantle dynamics beneath the south Pacific. Science 248 (4958), 969–975. http://dx.doi.org/10.1126/science.248.4958.969.

Morgan, W.J., 1972. Deep mantle convection plumes and plate motions. Am. Assoc. Pet. Geol. Bull. 56 (2), 203–213.

Müller, R.D., Sdrolias, M., Gaina, C., & Roest, W.R., 2008. Age, spreading rates, and spreading asymmetry of the World's ocean crust. Geochem. Geophys. Geosyst 9 (4), 1–19. http://dx.doi.org/10.1029/2007GC001743.

Nakanishi, M., 1993. Topographic expression of five fracture zones in the northwestern Pacific ocean. In: Pringle, M.S., Sager, W.W., Sliter, W.V., Stein, S. (Eds.), The Mesozoic Pacific: Geology, Tectonics and VolcanismGeophys. Monograph Ser. vol. 77. AGU, Washington, D.C., pp. 121–136. http://dx.doi.org/10.1029/GM077p0121.

Natland, J.H., 1976. Petrology of volcanic rocks dredged from seamounts in the Line Islands. Initial Rep. Deep Sea Drill. Proj. 33 (26), 749–777.

Parsons, B., & Sclater, J.G., 1977. An analysis of the variation of ocean floor bathymetry and heat flow with age. J. Geophys. Res. 82 (5), 803–827. http://dx.doi.org/10.1029/JB082i005p00803.

Sager, W.W., & Keating, B.H., 1984. Paleomagnetism of Line Islands seamounts: evidence for late Cretaceous and early Tertiary volcanism. J. Geophys. Res. 89 (B13), 11135–11151. http://dx.doi.org/10.1029/JB089iB13p11135.

Sandwell, D.T., & Smith, W.H.F., 2009. Global marine gravity from retracked Geosat and ERS-1 altimetry: ridge segmentation versus spreading rate. J. Geophys. Res. 114 (B01411). http://dx.doi.org/10.1029/2008JB006008.

Schlanger, S.O., Garcia, M.O., Keating, B.H., Naughton, J.J., Sager, W.W., Haggerty, J.A., Philpotts, J.A., & Duncan, R.A., 1984. Geology and geochronology of the Line Islands. J. Geophys. Res. 89 (B13), 11261–11272. http://dx.doi.org/10.1029/JB089iB13p11261.

Smith, W.H.F., 1993. On the accuracy of digital bathymetric data. J. Geophys. Res. 98 (86), 9591–9603.

Smith, W.H.F., & Sandwell, D.T., 1994. Bathymetry prediction from dense satellite altimetry and sparse shipboard bathymetry. J. Geophys. Res. 99, 21803–21824.

Smith, W.H.F., & Sandwell, D.T., 1997. Global seafloor topography from satellite altimetry and ship depth soundings. Science 277 (5334), 1956–1962. http://dx.doi.org/10.1126/science.277.5334.1956.

Stein, C.A., & Stein, S., 1992. A model for the global variation in oceanic depth and heat flow with lithospheric age. Nature 359, 123–129. http://dx.doi.org/10.1038/359123a0.

Walcott, R.I., 1970. Flexural rigidity, thickness, and viscosity of the lithosphere. J. Geophys. Res. 75 (20), 3941–3953. http://dx.doi.org/10.1029/JB075i020p03941.

Watts, A.B., 1978. An analysis of isostasy in the World's oceans: 1 Hawaiian-Emperor seamount chain. J. Geophys. Res. 83 (B12), 5989–6004. http://dx.doi.org/10.1029/JB083iB12p05989.

Watts, A.B., 2001. Isostasy and Flexure of the Lithosphere. Cambridge University Press, London.

Watts, A.B., Sandwell, D.T., Smith, W.H.F., & Wessel, P., 2006. Global gravity, bathymetry, and the distribution of submarine volcanism through space and time. J. Geophys. Res. 111 (B08408). http://dx.doi.org/10.1029/2005JB004083.

Wessel, P., 2001. Global distribution of seamounts inferred from gridded Geosat/ERS-1 altimetry. J. Geophys. Res. 106 (B9), 19431–19441. http://dx.doi.org/10.1029/2000JB000083.

Wilson, J.T., 1963. Evidence from islands on the spreading of ocean floors. Nature 197, 536–538. http://dx.doi.org/10.1038/197536a0.

Winterer, E.L., 1976. Bathymetry and regional tectonic settings of the Line Islands chain. Initial Rep. Deep Sea Drill. Proj. 33 (25), 731–748.

Zhang, J., Jin, X., Gao, J., & Zhao, L., 2006. Influence on the seamounts' formation in MPM and WPSP from fractures and cretaceous magma's activities. Mar. Geol. Quat. Geol. 26 (1), 67–74 (in Chinese with English abstract).